Available online at www.sciencedirect.com

ScienceDirect

International Journal of Solids and Structures 45 (2008) 3897–3907

INTERNATIONAL JOURNAL OF SOLIDS AND STRUCTURES

www.elsevier.com/locate/ijsolstr

# Brittle versus ductile transition of nanocrystalline metals

Fan Yang [a], Wei Yang [b,a,*]

[a] *Department of Engineering Mechanics, Tsinghua University, Beijing 100084, China*
[b] *Zhejiang University, Hangzhou 310058, China*

Received 6 May 2007; received in revised form 16 November 2007
Available online 10 January 2008

**Abstract**

The brittle versus ductile transition for conventional metals is dictated by the competition between dislocation emission and cleavage. For nanocrystalline metals with grain size below 25 nm, however, dislocation activities are suppressed and the classic theory fails to apply. In this paper, one of the competing mechanisms that control the brittle versus ductile transition of nanocrystalline metals is found to be the grain boundary dominated creep deformation versus the grain boundary decohesion. A model is proposed to quantify the crack propagation in nanocrystalline metals. The effects of material properties, initial configuration and applied loads on the property of crack propagation are addressed. It is concluded that either the increases in the initial crack length, the applied load and the grain boundary damage, or the deterrence in creep deformation, accelerate the crack propagation, and vice versa.


*Keywords:* Nanocrystalline metals; Brittle versus ductile transition; Grain boundary creep; Crack propagation

## 1. Introduction

Nanocrystalline metals have been widely studied (Gleiter, 1989; Meyers et al., 2006) for endeavors such as high strength and ductility since 1980s. However, several experiments (Karch et al., 1987; Koch et al., 1999) indicated that nanocrystalline metals frequently exhibited lower toughness and ductility than their coarse-grained counterparts. Accordingly, a clear understanding to the mechanism that controls the brittle versus ductile transition of nanocrystalline metals is of vital importance.

In conventional crystals, the brittle versus ductile transition is controlled by the competition between dislocation emission and cleavage (Rice and Thomson, 1974). When the grain size falls below 25 nm, however, experiments (Ke et al., 1995; Schuh et al., 2002) and theoretical analysis (Gryaznov, 1991) indicated that activities of dislocations were inhibited, and the classic mechanism for coarse-grained metals no longer applied. New mechanisms of the brittle versus ductile transition for nanocrystalline metals must be found.

* Corresponding author. Address: Department of Engineering Mechanics, Tsinghua University, Beijing 100084, China. Tel.: +86 10 6278 2642; fax: +86 10 6258 1824.
*E-mail addresses:* yangw@zju.edu.cn, yw-dem@tsinghua.edu.cn (W. Yang).

0020-7683/$ - see front matter © 2008 Elsevier Ltd. All rights reserved.
doi:10.1016/j.ijsolstr.2007.12.018

In the study on deformation mechanisms of nanocrystalline metals, MD simulations (Schiøtz and Jacobsen, 2003) and bubble rafts experiments (Van Vliet et al., 2003) suggested that the dislocation dominated deformation mechanism was replaced by the grain boundary dominated mechanism when the grain size was reduced to nanometers. A maximum strength is believed to exist for each category of grain sizes (Schiøtz and Jacobsen, 2003; Xiang and Guo, 2006). The softening effect for smaller grains could not be explained by the classical theory of dislocation induced plasticity, but rather the manifestation of grain boundary mechanism in nanocrystals. The classic theories such as Coble creep take into account the grain boundary diffusion and have a grain size correlation. But its prediction of elongated grain shape does not correlate with the experiment data of rolling nanocrystalline Cu (Lu et al., 2000), in which the grains keep equal-axial even at an extend of 5100% elongation. Meanwhile, grain rotation was observed in the experiment (Shan, 2004). Based on the experiments and analysis, Yang and Wang (2004) proposed a grain-cooperated deformation model (that included grain boundary sliding, grain boundary diffusion and grain rotation) to describe the grain boundary dominated deformation.

On the study of fracture process, the increase of grain boundary volume would raise the possibility for the crack to propagate through the grain boundaries. Indeed, experiments (Xiao et al., 2001; Kumar et al., 2003) and MD simulations (Farkas et al., 2002; Farkas et al., 2005; Frederiksen et al., 2004 revealed that crack propagation in nanocrystalline metals preferentially took the path along grain boundaries. The crack propagation is assisted by the cavitation along the grain boundaries and the triple junctions in front of the crack tip. The void formation was attributed to the inconsistency in grain-cooperated deformation (Kumar et al., 2003), as well as the impurities introduced in the synthesis process (Agnew et al., 2000). Experiments (Sanders et al., 1997; Lu et al., 2000; Agnew et al., 2000) reported that compact samples with fewer voids and impurities usually exhibited higher toughness and ductility prior to failure. The cavitation of the grain boundary controlled by the diffusion (as reviewed by Raj and Ashby, 1975) has a rate that has positive correlations to the grain boundary diffusivity and the applied load. The increased availability for the crack to extend along the grain boundaries and the diffusion enhanced grain boundary cavitation make the decohesion along grain boundaries a dominant mechanism for the failure of nanocrystalline metals.

Based on the existing researches, we regard the grain boundary dominated creep and grain boundary decohesion as two competing mechanisms that control crack propagation in nanocrystalline metals. The boundary dominated plastic deformation causes the crack to blunt and the stress near the crack tip to relax, while the grain boundary decohesion causes the crack to extend. If the former mechanism prevails, the material exhibits considerable ductility; while the material would behave brittle if the latter mechanism dominates. In this paper, a model to investigate the brittle to ductile transition of nanocrystalline metals is proposed to quantify the competition of two mechanisms.

## 2. Formulation and parameter dependence

### 2.1. Quantification of two competing mechanisms

A model for brittle versus ductile competition requires the quantification for two competing mechanisms of grain boundary dominated creep and grain boundary decohesion. The 9-grain cluster model proposed by Yang and Wang (2004) is adopted to characterize the deformation of nanocrystalline metals. The 9-grain cluster model incorporates both Ashby–Verrall mechanism (Ashby and Verrall, 1973) and the relative rotation of closely linked grain pairs. The insertion/rotation process features the creep deformation of nanocrystalline metals. In that model, the energy dissipation in the deformation process equals to the external working done on the sample:

$$\dot{W} = \dot{W}_{\text{diffusion}} + \dot{W}_{\text{slide}} + \dot{W}_{\text{GB}} + \dot{W}_{\text{disorder}} = \sigma\dot{\varepsilon} \tag{1}$$

Four terms that composing of $\dot{W}$ correspond to the energy dissipations through four mechanisms: the grain boundary mass diffusion, the grain boundary sliding, the fluctuation of grain boundary area and ordering/disordering transition, respectively. They are expressed as (Yang and Wang, 2004):

$$\dot{W}_{\text{diffusion}} = \frac{8m^2K_{\text{B}}TD^2}{3\sqrt{3}\Omega\left\{nD_{\text{v}} + D_{\text{B}}\sum_{i=1}^{n}\frac{\delta}{l_i}\right\}}\frac{\dot{\varepsilon}^2}{\Delta\varepsilon^2}, \quad \dot{W}_{\text{slide}} = \frac{8\eta_{\text{B}}}{\sqrt{3}\delta}Ds^2\dot{\varepsilon}^2/\Delta\varepsilon^2,$$
$$\dot{W}_{\text{GB}} = \left(\sqrt{2\sqrt{3}} - \sqrt{3}\right)\frac{4\Gamma}{3D}\frac{\dot{\varepsilon}}{\Delta\varepsilon}, \quad \dot{W}_{\text{disorder}} = \left(1 - \frac{\pi}{2\sqrt{3}}\right)\Delta g_0\frac{\dot{\varepsilon}}{\Delta\varepsilon} \tag{2}$$

where $m$ and $n$ are dimensionless parameters in diffusion, $K_{\text{B}}$ denotes the Boltzmann constant and $T$ the absolute temperature, $D$ is the grain diameter, $D_{\text{V}}$ and $D_{\text{B}}$ denote the diffusivity through lattice and through grain boundary, respectively, $\delta$ is the thickness of the disordered layer and $l_i$ the diffusion distance, $\eta_{\text{B}}$ is the viscosity coefficient and $s$ the dimensionless sliding quantity, $\Gamma$ denotes grain boundary energy per unit area, $\Delta g_0$ denotes the energy difference from the disordered to the ordered state, and $\Delta\varepsilon$ denotes the strain increment after a cycle of the deformation process. Various quantities $m$, $n$, $l_i$ and $s$ were tabulated by Yang and Wang (2004).

The creep law under that framework can be deduced as (Yang and Wang, 2004):

$$\dot{\varepsilon} = C(\sigma - \sigma_{\text{th}}) \tag{3}$$

where the creep rate coefficient $C$ and creep threshold stress $\sigma_{\text{th}}$ depend on the grain size, the temperature and the intrinsic material properties. The model agrees well with the low-temperature creep data of the electrodeposited nanocrystalline Cu (Cai et al., 2000). A full cycle of insertion/rotation for the deformation can be visualized as unfolding the grains located previously in zigzag lines to straight lines, as illustrated in Fig. 1.

With the presence of a crack, the evolution of the configuration with grain-cooperated deformation is illustrated in Fig. 2. As one may observe, the crack not only blunts but also subtracts laterally as the grain boundary dominated creep spreads the entire material under the applied load. The incompressibility dictates that the blunting rate, as well as the subtracting rate of the crack are in accordance with the creep rate of the surrounding materials, i.e.:

$$\frac{\dot{\delta}}{\delta} = -\frac{\dot{a}}{a} = \dot{\varepsilon} \tag{4}$$

In the case of constant remote stress, Eq. (4) can be integrated as:

$$\delta = \delta_0 e^{\dot{\varepsilon}(t-t_0)} = \delta_0 e^{C(\sigma_{\text{n}}-\sigma_{\text{th}})(t-t_0)}$$
$$a = a_0 e^{-\dot{\varepsilon}(t-t_0)} = a_0 e^{-C(\sigma_{\text{n}}-\sigma_{\text{th}})(t-t_0)} \tag{5}$$

where $\delta$ and $a$ are the crack width and the crack length, respectively, with their initial values $\delta_0$ and $a_0$ at time $t_0$.

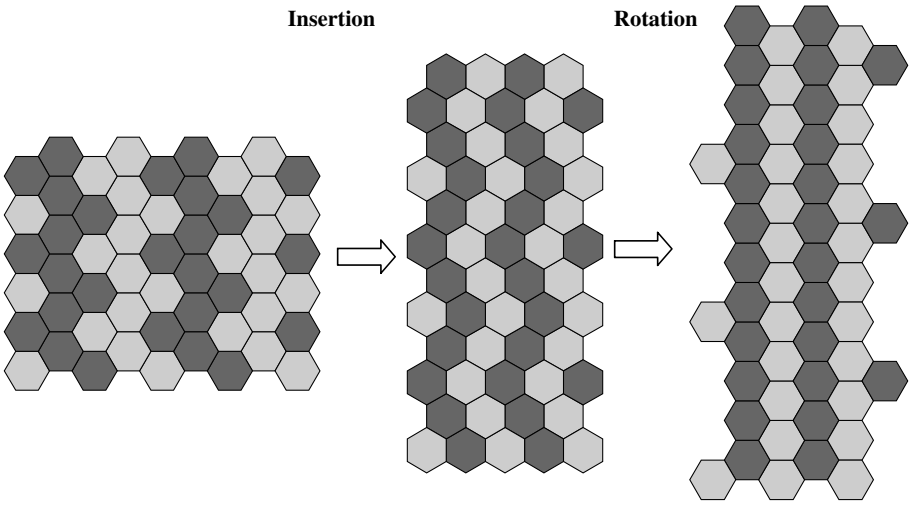


Fig. 1. Illustration of 9-grain cluster model as "fold lines to straight lines".

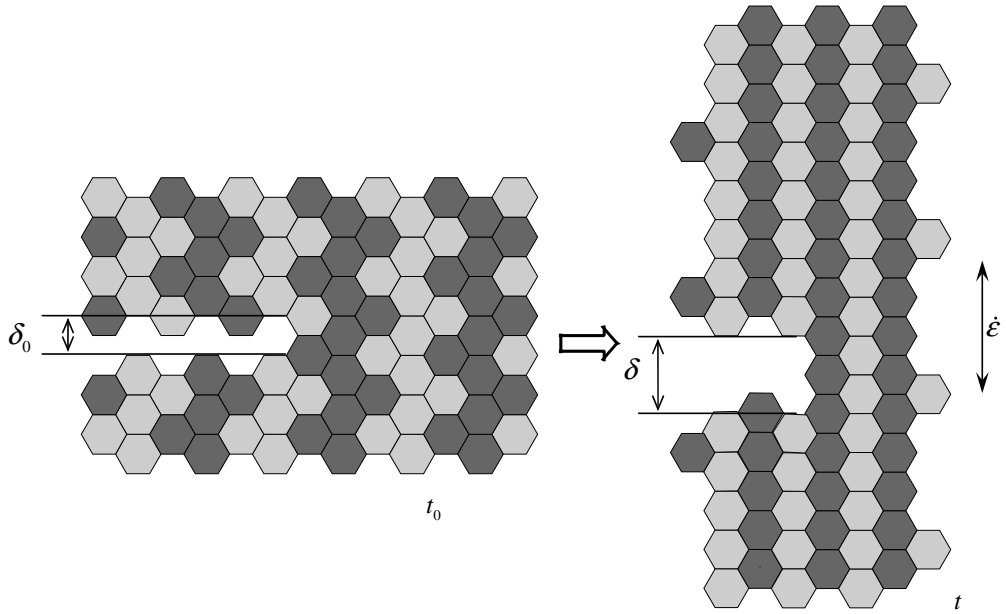


Fig. 2. Illustration of crack blunting due to grain-cooperated deformation.

For the mechanism of grain boundary decohesion, experiments and simulations showed that cavitation along grain boundaries in front of the crack tip is of vital importance. The process consists of the deposition of cavities and impurities along the grain boundaries during synthesis, the nucleation and growth of voids at the grain boundaries and triple junctions under applied load, the coalescence of voids to form micro-cracks and the connection of micro-cracks to a main crack, as illustrated in Fig. 3.

To quantify the mechanism of grain boundary decohesion assisted by void evolution, a damage variable $\omega$ is introduced which bears a physical meaning of the area percentage of cavitated grain boundary. The decohering process is formulated by damage evolution along grain boundaries. For simplicity, damage evolution is characterized by a power law, as an approximate expression for the diffusion controlled grain boundary cavitation process:

$$\dot{\omega} = \begin{cases} 0, & \sigma \leqslant \sigma_{\mathrm{dam}} \\ B\left(\frac{\sigma_{\mathrm{n}} - \sigma_{\mathrm{dam}}}{1-\omega}\right)^{v}, & \sigma > \sigma_{\mathrm{dam}} \end{cases} \tag{6}$$

where $\sigma_{\mathrm{n}}$ is the applied stress normal to the grain boundaries and $\sigma_{\mathrm{dam}}$ is the threshold stress for damage evolution. Integration of Eq. (6) leads to:

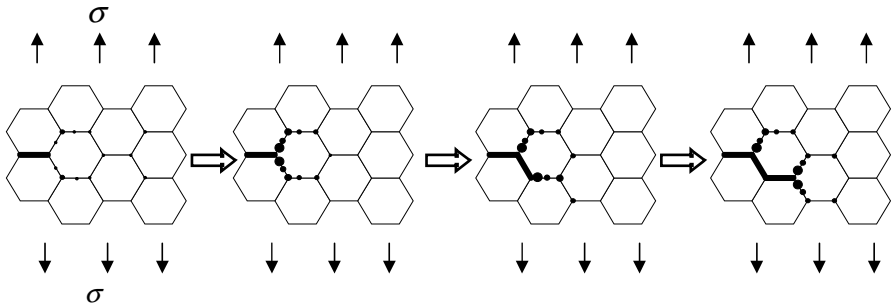


Fig. 3. Crack growth assisted by void evolution along grain boundaries.

$$\int_{t_0}^{t_1} \langle \sigma_n(t) - \sigma_{dam} \rangle^v dt = \frac{1}{B(1+v)} \tag{7}$$

where

$$\langle \sigma_n(t) - \sigma_{dam} \rangle = \begin{cases} 0, & \sigma \leqslant \sigma_{dam} \\ \sigma_n(t) - \sigma_{dam}, & \sigma > \sigma_{dam} \end{cases} \tag{8}$$

and $t_1$ refers to the instance that $\omega$ reaches the critical value of unity.

To consider the crack blunting effect of creep deformation, we adopt the simplified version of Neuber formula (Constable et al., 1970) for a notch configuration to express the stress distribution ahead of the crack tip. The stress normal to the plane of the crack midline can be expressed as:

$$\sigma_n = \sigma\left(\frac{2c}{a} + \frac{2\rho}{a}\right)\left(\frac{2c}{a} + \frac{\rho}{a}\right)^{-\frac{3}{2}} = \sigma_n\left(\frac{\rho}{a}, \frac{c}{a}\right) \tag{9}$$

where $\rho$ is the radius of curvature of the crack tip, $a$ is the crack length, $c$ is the distance from the crack tip and $\sigma$ is the remote stress. Under constant remote stress, the normal stress distribution depends on two dimensionless variables $\rho/a$ and $c/a$. Eq. (9) agrees with the stress field of linear elastic fracture mechanics when $\rho/a$ tends to zero.

### 2.2. A model to combine two competing mechanisms

A model is proposed to combine two mechanisms for the crack propagation process in nanocrystalline metals. The crack propagates due to grain boundary cavitation, and blunts due to grain boundary dominated creep. A segment of grain boundary decoheres only if every points of the segment reach the critical damage condition. Then, two adjacent grains depart from each other via cooperative deformation of grains. For simplicity, the real crack profile is neglected and the crack configuration is idealized as a straight line with the initial width of one grain diameter. The crack is assumed to propagate a length of one grain at each step. The process is illustrated in Fig. 4. The radius of curvature can be approximated as the circumradius of the crack tip profile as illustrated in Fig. 5.

Denote the instant of load application as $t_0$. The initial radius of curvature is taken as $\rho_0 = D/2$. Because the normal stress decreases as the point moves away from the crack tip, the requirement for the decohesion of grain boundary of length $D$ is equivalent to achieving critical damage at point $c = D$. The normal stress in front of the crack tip is assumed to be invariable during each propagation step.

Denote $t_i$ as the time at which the $i$th step of propagation is completed. The crack configuration after the $i$th propagation step is characterized by:

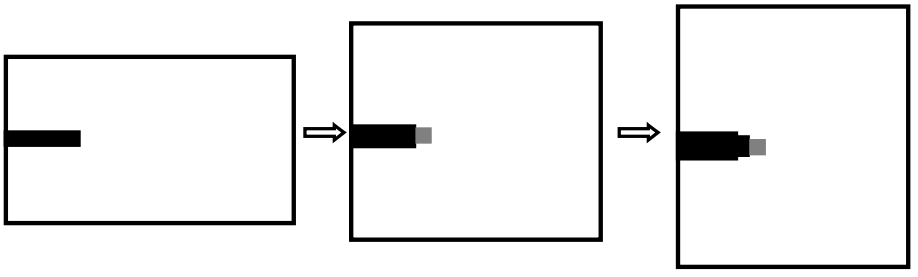

Fig. 4. A simplified model of crack propagation controlled by two competing mechanisms.

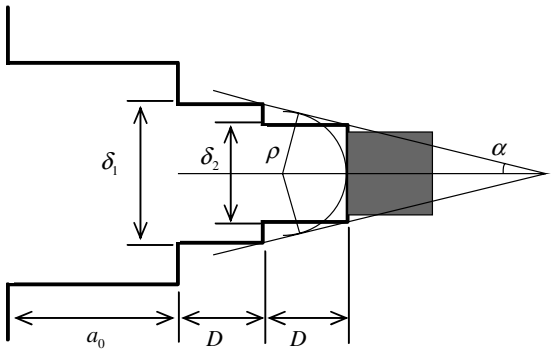


Fig. 5. Calculation for the radius of curvature at a crack tip.

$$a_i = a_0 \mathrm{e}^{-C(\sigma-\sigma_{\mathrm{th}})(t_i-t_0)} + \sum_{j=0}^{i-1}\left[D\prod_{k=j}^{i-1}\mathrm{e}^{-C(\sigma_{\mathrm{n}}(t_k)-\sigma_{\mathrm{th}})\Delta t_k}\right] \tag{10}$$

$$\rho_i = \frac{D}{2}\frac{1}{\sqrt{1+\tan^2\alpha_i}-\tan\alpha_i}$$

$$\tan\alpha_i = \frac{\mathrm{e}^{C(\sigma_{\mathrm{n}}(t_i)-\sigma_{\mathrm{th}})(t_i-t_{i-1})}-1}{2\mathrm{e}^{-C(\sigma_{\mathrm{n}}(t_i)-\sigma_{\mathrm{th}})(t_i-t_{i-1})}} \tag{11}$$

Based on the damage accumulation Eq. (7), one estimates the time cost for step $i+1$ of crack propagation as:

$$\Delta t_i = \frac{\frac{1}{B(1+v)} - \sum_{j=0}^{i-1}\Delta t_j\left\langle \sigma_{\mathrm{n}}\left(\frac{\rho_j}{a_j}, \frac{\sum_{k=j}^{i}\left(D\prod_{l=j+1}^{k}\mathrm{e}^{C(\sigma_{\mathrm{n}}(t_l)-\sigma_{\mathrm{th}})\Delta t_{l-1}}\right)}{a_j}\right) - \sigma_{\mathrm{dam}}\right\rangle^{v}}{\left\langle \sigma_{\mathrm{n}}\left(\frac{\rho_i}{a_i}, \frac{D}{a_i}\right) - \sigma_{\mathrm{dam}}\right\rangle^{v}} \tag{12}$$

$$t_{i+1} = t_i + \Delta t_i \tag{13}$$

The crack length at step $i$ may be converted to the initial configuration as:

$$\underline{a}_i = a_0 + \sum_{j=0}^{i-1}\left[D\prod_{k=0}^{j}\mathrm{e}^{C(\sigma_{\mathrm{n}}(t_k)-\sigma_{\mathrm{th}})\Delta t_k}\right] \tag{14}$$

provided that the effect of lateral contraction due to creep deformation is omitted.

### 2.3. Parameter dependence of crack propagation

We explore the dependence of the crack propagation speed on various parameters such as remote stress, creep coefficient and damage evolution coefficient. Repeating the calculations from Eqs. (10)–(14) for each propagation step, one obtains the time costs for each step, as well as the plots for crack length versus time.

Let us take the case of electro-deposited nanocrystalline Cu (Cai et al., 2000) for a model calculation. Experiment data furnished the creep coefficient $C$ of $6\,\mathrm{E}{-14}\,\mathrm{Pa}^{-1}\,\mathrm{s}^{-1}$ and creep threshold stress of 130 MPa for nanocrystalline Cu ($D = 30$ nm) at 310 K. The time scales for the GB cavitation and GB induced creep deformation are comparable since both involve GB diffusion. Thus, a magnitude relation of $C(\sigma_{\mathrm{n}}-\sigma_{\mathrm{th}}) \sim B(\sigma_{\mathrm{n}}-\sigma_{\mathrm{dam}})^v$ should hold ahead of the crack. Select a control point five grains ahead of the crack tip, one estimates $\sigma_{\mathrm{n}}$ as 1000 MPa under the values of $a_0 = 500D$ and $\sigma = 150$ MPa. Take $v$ as 1.5, $\sigma_{\mathrm{dam}}$ as 200 MPa, the magnitude of $B$ is estimated as $2\,\mathrm{E}{-18}\,\mathrm{Pa}^{-3/2}\,\mathrm{s}^{-1}$.

To investigate the effect of remote stress $\sigma$, one may vary $\sigma$ in five levels: 50, 70, 100, 150 and 200 MPa, ranging from the case of small scale yielding to that of global yielding. While the other parameters are fixed as $C = 6\,\mathrm{E}{-14}\ \mathrm{Pa}^{-1}\ \mathrm{s}^{-1}$, $\sigma_{\mathrm{th}} = 130$ MPa, $B = 2\,\mathrm{E}{-18}\ \mathrm{Pa}^{-3/2}\ \mathrm{s}^{-1}$, $\sigma_{\mathrm{dam}} = 200$ MPa, $v = 1.5$ and $a_0 = 500D$. The results are shown in Fig. 6. Fig. 6(c) is an enlarged view for the short time response exhibited in Fig. 6(b). That graph exhibits the interesting variation of crack length from the initial contraction (by blunting and lateral subtraction) to the subsequent elongation. This phenomenon is attributed to the fact that the first few steps of crack growth cost much longer time than the subsequent ones, as shown in Fig. 6(a), and that favors the lateral contraction due to GB induced creep. It is also noted that a higher remote stress causes more evident lateral contraction. Subtracting the lateral contraction effect, as shown in Fig. 6(d), one observes that the growth rate of the crack rises monotonically with the remote stress.

To investigate the effect of creep coefficient $C$, one may vary $C$ to four levels of $3\,\mathrm{E}{-14}\ \mathrm{Pa}^{-1}\ \mathrm{s}^{-1}$, $6\,\mathrm{E}{-14}\ \mathrm{Pa}^{-1}\ \mathrm{s}^{-1}$, $9\,\mathrm{E}{-14}\ \mathrm{Pa}^{-1}\ \mathrm{s}^{-1}$, $12\,\mathrm{E}{-14}\ \mathrm{Pa}^{-1}\ \mathrm{s}^{-1}$, respectively, while the other parameters are set as: $\sigma = 150$ MPa, $\sigma_{\mathrm{th}} = 130$ MPa, $B = 2\,\mathrm{E}{-18}\ \mathrm{MPa}^{-3/2}\ \mathrm{s}^{-1}$, $\sigma_{\mathrm{dam}} = 200$ MPa, $v = 1.5$ and $a_0 = 500D$. The results are plot in Fig. 7. Fig. 7(b) clearly indicates that the crack propagation is slower and the lateral contraction effect is more prominent as the creep coefficient $C$ increases.

Attention is then focused on the effect of damage evolution coefficient $B$ by choosing the latter in four different values of $1\,\mathrm{E}{-18}$, $2\,\mathrm{E}{-18}$, $3\,\mathrm{E}{-18}$ and $4\,\mathrm{E}{-18}\ \mathrm{Pa}^{-3/2}\ \mathrm{s}^{-1}$. Other parameters are fixed as: $\sigma = 150$ MPa, $C = 6\,\mathrm{E}{-8}\ \mathrm{MPa}^{1-}\ \mathrm{s}^{-1}$, $\sigma_{\mathrm{th}} = 130$ MPa, $\sigma_{\mathrm{dam}} = 200$ MPa, $v = 1.5$ and $a_0 = 500D$. The results are shown in Fig. 8. A high value of damage evolution coefficient $B$ strives to accelerating crack propagation.

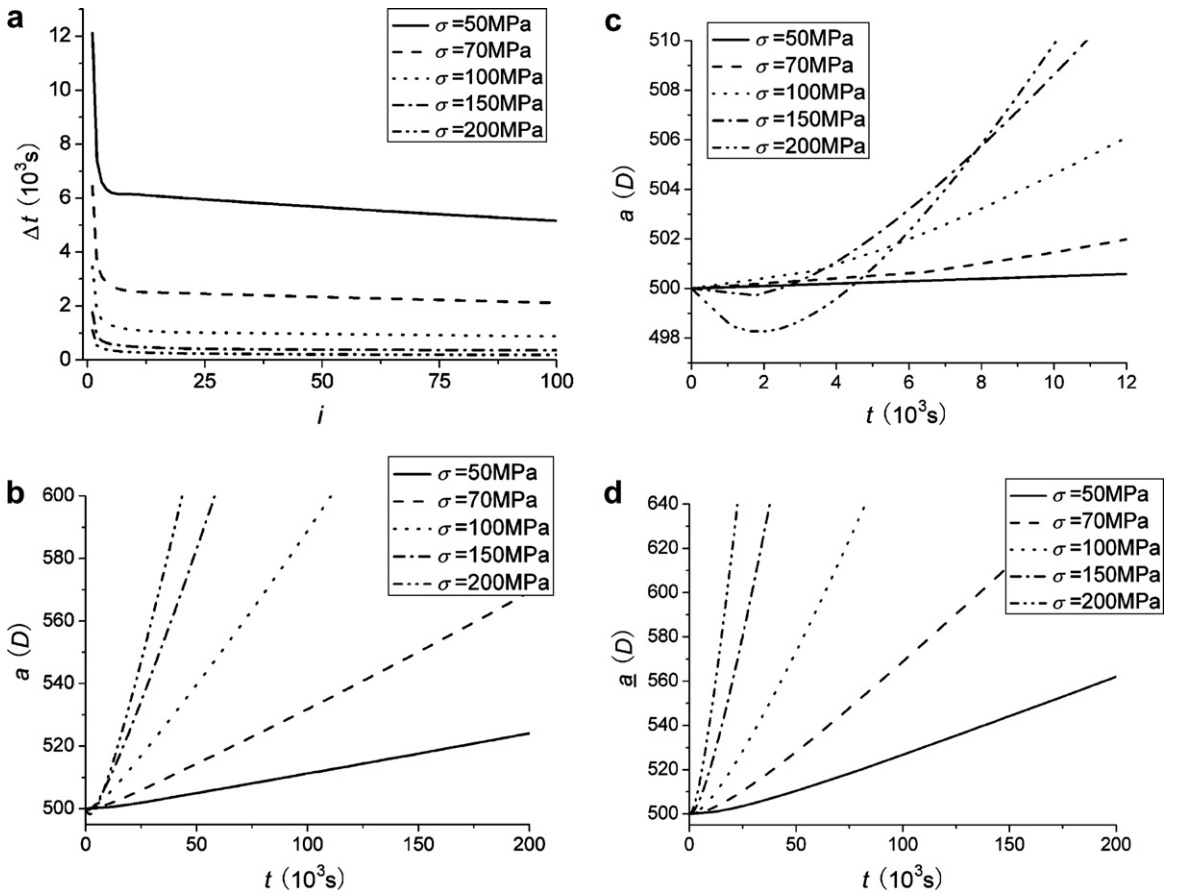


Fig. 6. Effect of remote stress on crack propagation. (a) Time cost for each propagation step; (b) crack length versus time; (c) a close-up view of (b) for the short time response that delineates the initial contraction of the crack; and (d) crack length versus time (with the lateral contraction effect subtracted).

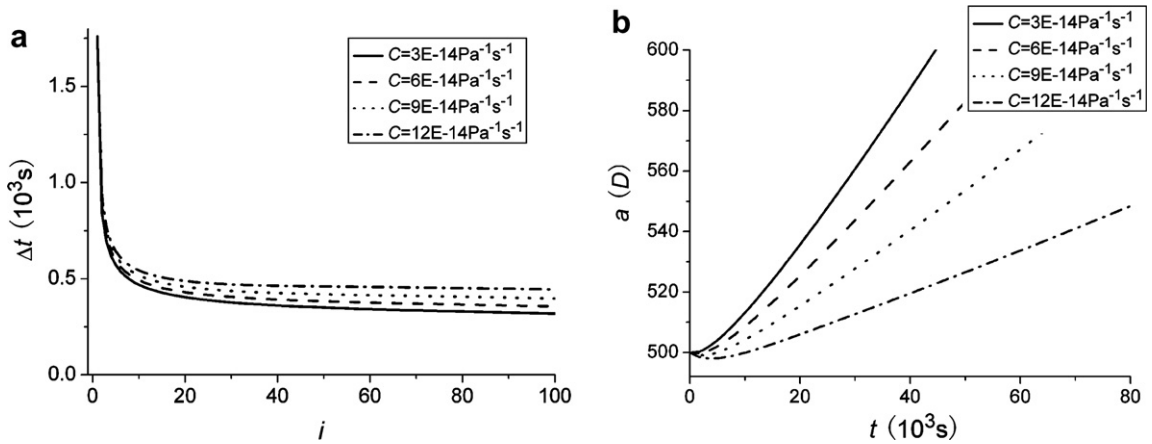


Fig. 7. Effect of creep rate coefficient on crack propagation. (a) Time cost for each propagation step and (b) crack length versus time.

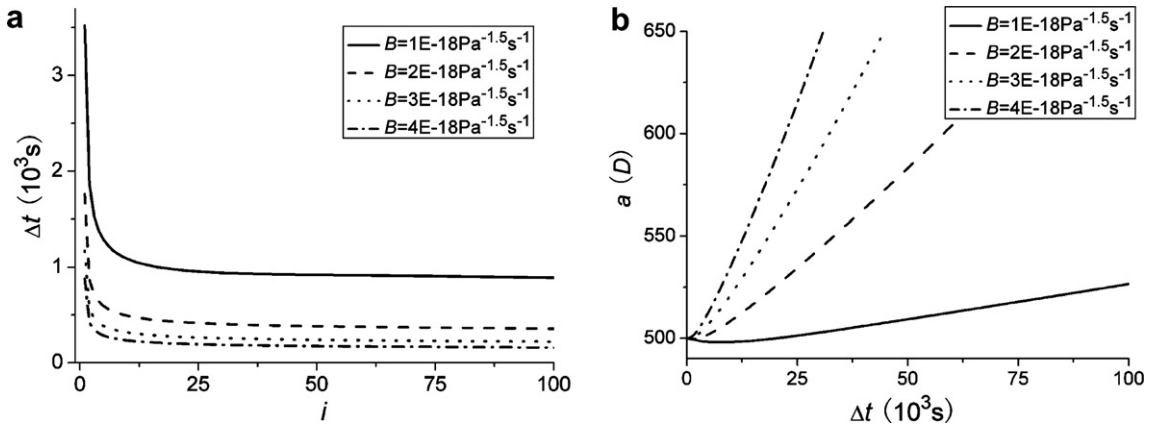


Fig. 8. Effect of grain boundary damage rate coefficient on crack propagation. (a) Time cost for each propagation step and (b) the crack length versus time.

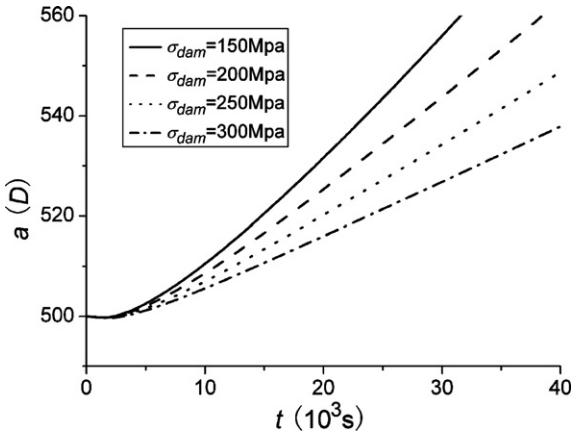


Fig. 9. Effect of threshold stress for damage evolution on crack propagation.

As for the effect of the threshold stress of damage evolution $\sigma_{\text{dam}}$, four values are chosen: 150, 200, 250 and 300 MPa. Other parameters are set as: $\sigma = 150$ MPa, $C = 6\text{E}{-}14\ \text{Pa}^{-1}\ \text{s}^{-1}$, $\sigma_{\text{th}} = 130$ MPa, $B = 2\text{E}{-}18\ \text{Pa}^{-3/2}\ \text{s}^{-1}$, $v = 1.5$ and $a_0 = 500D$. The results are shown in Fig. 9. A high value of threshold stress suppresses the damage evolution, and consequently deters the crack propagation.

## 3. Criterion of crack initiation

Attention is now focused on the initiation of crack growth after the load is imposed. As shown in Section 2.3, the first propagation step costs much longer time than the subsequent ones do. Once the crack propagation starts, its growth rate increases with time. Thus, the point of crack initiation is critical for the brittle versus ductile transition. The above assumption that stress distribution retains constant during each propagation step is rather crude for the calculation of crack initiation, since the incubation time for the first step is quite long. Referred to Eq. (7), the precise equation to calculate the incubation time for crack initiation is:

$$\int_0^{t_1} \left\langle \frac{\sigma\left(\frac{2D}{a_0}\mathrm{e}^{C(\sigma-\sigma_{\text{th}})t_1} + \frac{D}{a_0}\mathrm{e}^{2C(\sigma-\sigma_{\text{th}})t}\right)}{\left(\frac{2D}{a_0}\mathrm{e}^{C(\sigma-\sigma_{\text{th}})t_1} + \frac{D}{2a_0}\mathrm{e}^{2C(\sigma-\sigma_{\text{th}})t}\right)^{\frac{3}{2}}} - \sigma_{\text{dam}} \right\rangle^{v} \mathrm{d}t = \frac{1}{B(1+v)} \tag{15}$$

Introducing four dimensionless variables

$$\varepsilon_1 = C(\sigma - \sigma_{\text{th}})t_1, \quad A = \frac{C(\sigma - \sigma_{\text{th}})}{B\sigma^v}, \quad \tilde{a}_0 = \frac{a_0}{D}, \quad \tilde{\sigma}_{\text{dam}} = \frac{\sigma_{\text{dam}}}{\sigma} \tag{16}$$

one may convert Eq. (15) into the following dimensionless form:

$$(1+v)\int_0^{\varepsilon_1} \left\langle \frac{\tilde{a}_0^{1/2}(2\mathrm{e}^{\varepsilon_1} + \mathrm{e}^{2\varepsilon})}{\left(2\mathrm{e}^{\varepsilon_1} + \frac{1}{2}\mathrm{e}^{2\varepsilon}\right)^{\frac{3}{2}}} - \tilde{\sigma}_{\text{dam}} \right\rangle^{v} \mathrm{d}\varepsilon = A \tag{17}$$

The equation indicates that $\varepsilon_1$ is related to four independent dimensionless variables: $A$, $\tilde{a}_0$, $\tilde{\sigma}_{\text{dam}}$ and $v$. The four dimensionless quantities bear their own physical meanings. The value of $\varepsilon_1$ denotes the remote logarithmic strain at the crack initiation and that sets an upper limit for the integration variable $\varepsilon = C(\sigma - \sigma_{\text{th}})t$. The value of $A$ measures the ratio of the creep deformation to the deformation that induced by grain boundary damage evolution. The quantities $\tilde{a}_0$ and $\tilde{\sigma}_{\text{dam}}$ are the dimensionless initial crack length and dimensionless creep threshold stress.

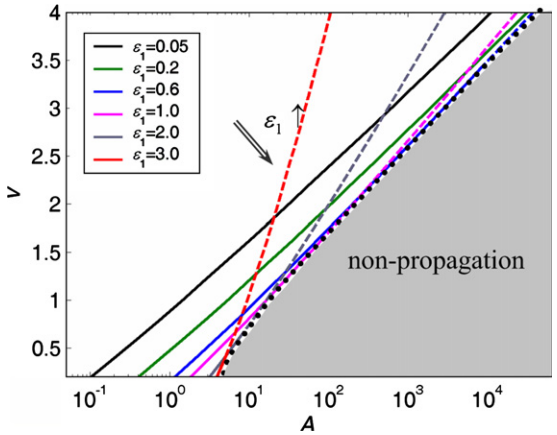


Fig. 10. Contour lines of $\varepsilon_1$ on the $A$–$v$ plane ($\tilde{a}_0 = 500, \tilde{\sigma}_{\text{dam}} = 2$), the dashed line indicates the artificial value of $\varepsilon_1$ at each relevant $A$–$v$ point, the black dotted line indicates the borderline between the propagation region and non-propagation region, the gray area indicates the non-propagation region.

Set $\tilde{a}_0 = 500$ and $\tilde{\sigma}_{\text{dam}} = 2$, the contour lines of $\varepsilon_1$ are plotted on the $A$–$v$ plane as in Fig. 10. It can be seen that $\varepsilon_1$ increases as $A$ increases or as $v$ decreases, indicating more work is required for the crack to propagate. There are two $\varepsilon_1$ values referring to each $A$–$v$ point. The larger one is artificial because the crack starts to extend as soon as the smaller $\varepsilon_1$ is reached. When the other parameters remain fixed, $A$ is observed to have a maximum value $A_{\max}$ as $\varepsilon_1$ takes different values. That fact can be interpreted as the existence of an envelop line. Beyond that envelop, a finite value of $\varepsilon_1$ is impossible, namely the crack does not propagate but only blunts. That envelop is shown by the bold dot line in Fig. 10, below which lies the non-propagation region. From Eq. (17), crack propagation is possible if and only if:

$$A < A_{\max} = \max_{\varepsilon_1}\left((1+v)\int_0^{\varepsilon_1}\left\langle \frac{\tilde{a}_0^{1/2}(2e^{\varepsilon_1}+e^{2\varepsilon})}{\left(2e^{\varepsilon_1}+\frac{1}{2}e^{2\varepsilon}\right)^{\frac{3}{2}}} - \tilde{\sigma}_{\text{dam}}\right\rangle^{v} d\varepsilon\right) \tag{18}$$

Either decreasing $v$ or $\tilde{a}_0$, or increasing $\tilde{\sigma}_{\text{dam}}$, can reduce $A_{\max}$, and consequently alter the brittle versus ductile transition. When

$$\frac{\tilde{\sigma}_{\text{dam}}}{\tilde{a}_0^{1/2}} > \frac{(2e^0+e^0)}{\left(2e^0+\frac{1}{2}e^0\right)^{\frac{3}{2}}} = 0.76 \tag{19}$$

one has $A_{\max} = 0$, and henceforth terminates the crack growth. Under general circumstances, Eq. (18) has no simplification. However, when $\tilde{\sigma}_{\text{dam}}/\tilde{a}_0^{1/2} \ll 1$, as in the case of a macroscopic crack, Eq. (18) can be reduced to:

$$A_{\max} \approx (1+v)\tilde{a}_0^{v/2}\max_{\varepsilon_1}\left(\frac{\varepsilon_1(2e^{\varepsilon_1}+1)^{v}}{(2e^{\varepsilon_1}+1/2)^{\frac{3}{2}v}}\right) \approx \left(\frac{\tilde{a}_0}{2}\right)^{\frac{v}{2}} \tag{20}$$

The $\varepsilon_1$ value for $A_{\max}$ varies approximately from 2 to 0.4 as $v$ varies from 1 to 4.

## 4. Conclusions

The brittle versus ductile transition in nanocrystalline metals with grain size below 25 nm is modeled quantitatively via the competing mechanisms of grain boundary decohesion versus grain boundary dominated creep. The model predicts the dependence of crack growth rate and crack initiation of nanocrystalline metals on material properties, initial configuration and applied loads. The crack propagates more rapidly under a larger remote stress, a higher damage evolution coefficient and a smaller creep coefficient. The remote logarithmic strain at crack initiation increases as the creep deformation mechanism overwhelms the grain boundary damage evolution mechanism. When the parameters of material properties, initial configuration and applied load satisfy a condition stated in Eq. (18), the crack will not propagate but only blunt. The non-propagation regime can be quantified by four dimensionless parameters as $A < A_{\max}(v, \tilde{a}_0, \tilde{\sigma}_{\text{dam}})$.

There has not yet been enough experiment data reported on the crack propagation of nanocrystalline metals to validate the present theory. However, the model introduced in this paper evaluates the relative effects of different parameters on the crack propagation, and suggests a tractable approach to predict the brittle versus ductile transition in nanocrystalline metals.

## Acknowledgements

This work is supported through grants by the 973 Projects of China (No. 2004CB619304) and also from the National Natural Science Foundation of China (Nos. 10332020 and 10121202).

## References

Ashby, M.F., Verrall, R.A., 1973. Diffusion-accommodated flow and superplasticity. Acta Metall. 21, 149–163.

Agnew, S.R., Elliott, B.R., Youngdahl, C.J., Hemker, K.J., Weertman, J.R., 2000. Microstructure and mechanical behavior of nanocrystalline metals. Mater. Sci. Eng. A 285, 391–396.

Cai, B., Kong, Q.P., Lu, L., Lu, K., 2000. Low temperature creep of nanocrystalline pure copper. Mater. Sci. Eng. A 286, 188–192.
Constable, I., Culver, L.E., Wlliams, J.G., 1970. Notch root radii effects in the fatigue of polymers. Int. J. Fract. Mech. 6, 279–285.
Farkas, D., Van Swygenhoven, H., Derlet, P.M., 2002. Intergranular fracture in nanocrystalline metals. Phys. Rev. B 66, 060101-1–060101-4.
Farkas, D., Petegem, S.V., Derlet, P.M., Swygenhoven, H.V., 2005. Dislocation activity and nano-void formation near crack tips in nanocrystalline Ni. Acta Mater. 53 (11), 3115–3123.
Frederiksen, S.L., Jacobsen, K.W., Schiøtz, J., 2004. Simulations of intergranular fracture in nanocrystalline molybdenum. Acta Mater. 52, 5019–5029.
Gleiter, H., 1989. Nanocrystalline materials. Prog. Mater. Sci. 33, 223–315.
Gryaznov, V.G., 1991. Size effects of dislocation stability in nanocrystals. Phys. Rev. B 44 (1), 42–46.
Karch, J., Birringer, R., Gleiter, H., 1987. Ceramics ductile at low temperature. Nature 330, 556–558.
Ke, M., Hackney, S.A., Milligan, W.W., Aifantis, E.C., 1995. Observation and measurement of grain rotation and plastic strain in nanostructured metal thin films. NanoStruct. Mater. 5, 689–697.
Koch, C.C., Morris, D.G., Lu, K., Inoue, A., 1999. Ductility of nanostructured materials. MRS Bull. 24, 54–58.
Kumar, K.S., Suresh, S., Chisholm, M.F., Horton, J.A., Wang, P., 2003. Deformation of electrodeposited nanocrystalline nickel. Acta Mater. 51, 387–405.
Lu, L., Sui, M.L., Lu, K., 2000. Superplastic extensibility of nanocrystalline copper at room temperature. Science 287, 1463–1466.
Meyers, M.A., Mishra, A., Benson, D.J., 2006. Mechanical properties of nanocrystalline materials. Prog. Mater. Sci. 51, 427–556.
Raj, R., Ashby, M.F., 1975. Intergranular fracture at elevated temperature. Acta. Metall. 23, 653–666.
Rice, J.R., Thomson, R., 1974. Ductile versus brittle behavior of crystals. Phil. Mag. 29, 73–97.
Sanders, P.G., Eastman, J.A., Weertman, J.R., 1997. Elastic and tensile behavior of nanocrystalline copper and palladium. Acta Mater. 45, 4019–4025.
Schiøtz, J., Jacobsen, K.W., 2003. A maximum in the strength of nanocrystalline copper. Science 301, 1357–1359.
Schuh, C.A., Nieh, T.G., Yamasaki, T., 2002. Hall-Petch breakdown manifested in abrasive wear resistance of nanocrystalline nickel. Scripta Mater. 46, 735–740.
Shan, Z., 2004. Grain boundary-mediated plasticity in nanocrystalline nickel. Science 305, 654–657.
Van Vliet, K.J., Tsikata, S., Suresh, S., 2003. Model experiments for direct visualization of grain boundary deformation in nanocrystalline metals. Appl. Phys. Lett. 83, 1441–1443.
Xiao, C., Mirshams, R.A., Whang, S.H., Yin, W.M., 2001. Tensile behavior and fracture in nickel and carbon doped nanocrystalline nickel. Mater. Sci. Eng. A 301, 35–43.
Xiang, Q., Guo, X., 2006. The scale effect on the yield strength of nanocrystalline materials. Int. J. Sol. Struct. 43, 7793–7799.
Yang, W., Wang, H.T., 2004. Mechanics modeling for deformation of nano-grained metals. J. Mech. Phys. Solids 52 (4), 875–889.